Monte Carlo Simulation of Atmospheric Radiative Forcings Using A Path-Integral Formulation Approach for Spectro-Radiative Sensitivities

Mourtaday Nada, Mégane Bati, Stéphane Blanco, Jean-Louis Dufresne, Mouna El-Hafi, Vincent Eymet, Vincent Forest, Richard Fournier, Jacques Gautrais, Paule Lapeyre, et al.

Monte Carlo simulation of atmospheric radiative forcings using a path-integral formulation approach for spectro-radiative sensitivities

Nada Mourtaday [a,*], Mégane Bati [a], Stéphane Blanco [a], Jean-Louis Dufresne [b], Mouna El Hafi [a,c], Vincent Eymet [d], Vincent Forest [d], Richard Fournier [a], Jacques Gautrais [e,a], Paule Lapeyre [f], Yaniss Nyffenegger-Péré [a], Najda Villefranque [g]

[a] *LAPLACE, Université de Toulouse, CNRS, INPT, UPS, Toulouse, France*
[b] *LMD/IPSL, Sorbonne Université, CNRS, École Polytechnique, ENS, Paris, France*
[c] *Université de Toulouse, Mines Albi, UMR 5302 - Centre RAPSODEE, Campus Jarlard, F-81013, Albi CT cedex 09, France*
[d] *Méso-Star, Toulouse, France*
[e] *CRCA, CBI, Université de Toulouse, CNRS, Toulouse, France*
[f] *Department of Mechanical and Mechatronics Engineering, University of Waterloo, 200 University Ave. W, Waterloo ON, Canada*
[g] *Centre National de Recherches Météorologiques, UMR 3589 CNRS, Météo France, Toulouse, France*

Keywords:
Line-by-line sampling
Radiative forcing
TOA flux sensitivity
HITRAN database
Radiative transfer
Monte Carlo

ABSTRACT

We present recent advances in path-integral formulations designed for unbiased Monte Carlo sensitivity estimation (in the form of partial derivatives) within a coupled physics model. We establish the theoretical foundation and illustrate the approach by estimating instantaneous atmospheric radiative forcings. In climate studies, these quantities amount for the change in top-of-atmosphere (TOA) net radiative flux induced by an isolated change in surface or atmospheric constitution. Based on a path-integral framework, our approach results in estimations consistent with well-established radiative forcings in the climate community. We highlight how physics coupling through path-integral formulations yields unbiased sensitivity estimation of a radiative quantity (integrated TOA flux) to a spectroscopic parameter (fraction change in gas concentration). Furthermore, we emphasize the method's scalability, demonstrating its compatibility with computer science acceleration techniques. These latter play a key role in rendering the computational time weakly sensitive to the system's multidimensional and multiphysics complexity.

Contents

1. Introduction and context

Monte Carlo methods yield unbiased estimates of integral quantities and their uncertainties, and as such, they have been employed for decades to provide reference results in atmospheric radiative transfer studies. Although being extensively used for benchmarking faster 1D radiative transfer codes to guide improvements in remote sensing, weather forecast and climate modeling, the high computational cost of Monte Carlo 3D codes, such as the I3RC community model [1] or MYSTIC [2], usually prevents their direct employment in operational contexts. However, recent transfer from computer science acceleration techniques to atmospheric radiative transfer science — to handle complex surfaces and detailed cloud fields for instance [3–5] — open new perspectives for using Monte Carlo methods beyond reference simulations. Indeed, these methods have recently been shown to be key in addressing multiphysics and multidimensional integrals [6] resulting in computationally efficient simulations that are insensitive to the size and complexity of the integration domains [5,7,8].

A recent example in this respect is a novel work that couples a line-by-line spectroscopic model to a radiative transfer model, resulting in a spectro-radiative model first described in [9], that has recently benefited from a close collaboration between multiple communities (computer science, atmospheric science, spectroscopy and radiative transfer physics). This collaboration has resulted in a Monte Carlo radiative transfer code specifically designed to estimate integrated radiative fluxes. Developed during the PhD work of Nyffenegger-Péré [10], it provides reference results for estimating atmospheric radiative fluxes integrated over any spatial, temporal and wavenumber domain, using the atmosphere and the surface properties' description as input data, typically derived from a global and multi-decadal General Circulation Model (GCM) simulation. A concrete application of this tool in climate science is estimating the global broadband flux at TOA, that is, radiances averaged temporally over a climate period and spatially over the whole globe, as well as integrated over all frequencies and outgoing directions, without any compromise on the radiative or the spectroscopic physics description. Moreover, the approach combines path-integral Monte Carlo methods — insensitive to the integration domains — with computer graphics acceleration techniques [11–13] — that guarantee fast convergence —, resulting in computation times of just a few seconds that are insensitive to the input data complexity. Consequently, the computational cost for estimating the radiative flux integrated over an entire century, the entire globe, and the entire infrared spectrum is comparable to the cost for one particular time, location, and wavenumber, for the same precision level [14].

As the partial derivatives of an integral quantity are themselves integrals, initial developments for constructing path-integral sensitivities have been available for about 20 years [15], offering the benefit of providing uncertainties for these estimates. Since then, multiple studies [16–19] have demonstrated that if we can estimate a quantity through Monte Carlo methods, then we also know how to estimate its sensitivities using these methods. However, statistical convergence issues often arise when estimating sensitivities in a manner specific to each application, making them at the heart of active fields of research, including computer graphics science [16]. Now, instantaneous radiative forcing — precisely the quantity we aim to estimate without bias from the perspective of the spectro-radiative model — can be determined in specific instances through sensitivity estimates, as illustrated in Section 3 for carbon dioxide concentrations. The instantaneous radiative forcing with respect to a parameter is defined as the variation in the outgoing radiative flux at TOA when this parameter value is changed while keeping the other physics model parameters fixed. Indeed, analyzing the physical mechanisms of global warming requires characterizing its evolution as a function of the climate system state. A first step is often to evaluate the radiative forcing resulting from a change in surface or atmospheric constitution (*e.g.*, gas, cloud, aerosol, or surface properties), which are parameters in the spectro-radiative model. Instead of computing two estimates based on different sets of parameter values for a finite differences estimation, sensitivities can be estimated using the straightforward path-integral Monte Carlo methods that differentiate the spectro-radiative model. The unbiased nature of these estimations on both the modeling level (through the path-integral formulation for physics coupling) and the simulation level (through Monte Carlo methods) is crucial. Indeed, the presence of approximations in the treatment of radiative transfer or spectroscopic processes introduces disparities in the forcings computed by different climate models [20,21]. Therefore, in the present work, we argue that in addition to estimating the radiative flux at TOA, we can build upon the spectro-radiative model framework to yield sensitivity estimates to any parameters of interest.

Section 2 serves as the theoretical framework of our approach, structured into three segments. In Section 2.1, which primarily serves as a recapitulation of previous works [9,10,14], we provide a succinct examination of the difficulties associated with calculating radiance. Next, we outline the path-integral foundations of its efficient Monte Carlo estimation through the null-collision technique [22]. Moving to Section 2.2, we establish a transport model for sensitivities that forms the core of our proposition here. This model shares strong physical similarities with the transport of radiance. As a result, it is shown that the theoretical advancements presented for estimating radiance can also be applied to estimate sensitivities and thus radiative forcings. In Section 2.3, the Monte Carlo simulation algorithm associated with the resulting sensitivity path-integral is detailed. This lays the groundwork for an in-depth discussion of the sensitivity results in Section 3.

2. Theory and methods

2.1. Estimating global outgoing radiative flux at TOA

The global outgoing radiative flux at TOA, $\bar{\phi}$, is the monochromatic radiance L_ν averaged over a time period Δt (typically 1 to 30 years), over the entire globe of area S, and integrated over all frequencies ν and outgoing directions $\vec{u}$:

$$\bar{\phi} = \frac{1}{S\Delta t}\int_{\Delta t} dt \int_S dS(\vec{x}) \int_0^{+\infty} d\nu \int_{2\pi} d\vec{u}\,|\vec{u}\cdot\vec{n}|\,L_\nu(\vec{x},\vec{u},t) \tag{1}$$

That can easily be reformulated as the following multivariate integral:

$$\bar{\phi} = \int_{\Delta t} p_T(t)dt \int_S p_S(\vec{x})dS(\vec{x}) \int_0^{+\infty} p_N(\nu)d\nu \int_{2\pi} p_U(\vec{u})d\vec{u} \left\{ \frac{\pi L_\nu(\vec{x},\vec{u},t)}{p_N(\nu)} \right\} \tag{2}$$

Provided that functions $p_T(t)$, $p_S(\vec{x})$, $p_N(\nu)$ and $p_U(\vec{u})$ are normalized over their respective domains of definition, this multivariate integral can be formulated as the expectancy of a random variable $\mathfrak{V}$ of realizations noted ω. $\bar{\phi}$ can therefore be estimated using a Monte Carlo algorithm that uses the following probability density functions (PDFs) for sampling:

- $p_T(t) = 1/\Delta t$ is a uniform probability density function used to sample values of time t over the $[t_0, t_0 + \Delta t]$ range,
- $p_S(\vec{x}) = 1/S$ is a uniform probability density function used to sample positions $\vec{x}$ over the surface S of a sphere that represents the Earth's TOA,

- $p_N(\nu)$ is a probability density function used to sample values of frequency ν over the $[0, +\infty[$ range. Employing importance sampling to account for frequencies in proportion to their contributions, we choose a probability density function that follows the Planck function, expressed for the maximal temperature encountered in the system T_{max}. Since $\int_0^{+\infty} L_\nu^{eq} d\nu = \sigma T_{max}^4 / \pi$, we choose $p_N(\nu) = (\pi L_\nu^{eq})/\sigma T_{max}^4$,
- $p_U(\vec{u}) = |\vec{u}.\vec{n}|/\pi$ is the probability density function used to sample an outgoing direction $\vec{u}$ over the upper hemisphere following Lambertian emission.

Eq. (2) unfolds as a linearly nested sequence of integrals over time, space, frequency, and direction. Consequently, using the *double randomization* principle [23,24], a *single* Monte Carlo iteration for this multivariate integral requires only a *single* sampling over *each* of the probability density functions. To break it down, one Monte Carlo realization of $\bar{\phi}$ involves sequentially sampling a time t over $[0, \Delta t]$ according to $p_T(t)$, a position $\vec{x}$ over S according to $p_S(\vec{x})$, a frequency ν over $[0, +\infty[$ according to $p_N(\nu)$ and a direction $\vec{u}$ over the outgoing hemisphere at $\vec{x}$ according to $p_U(\vec{u})$. The retained weight of the realization is then $\omega = \pi L_\nu(\vec{x}, \vec{u}, t)/p_N(\nu)$, of variance $\mathrm{Var}(\mho)$. According to the Central Limit Theorem, performing a large number of realizations N, their sample mean is a random variable $\bar{\mho}$, of realizations noted $\bar{\omega}$ which follows a normal distribution of variance $\mathrm{Var}(\bar{\mho}) = \mathrm{Var}(\mho)/N$. As a realization of $\bar{\mho}$, the sample mean $\bar{\omega}$ is an unbiased estimator for $\bar{\phi}$, for which $\mathrm{Var}(\bar{\mho})/(N-1)$ is an unbiased estimator for variance.

In practice, the monochromatic radiance field $L_\nu(\vec{x}, \vec{u}, t)$ is unknown. If the expression for L_ν within a heterogeneous and anisothermal participating medium can be formulated as a path integral, easily implementable using Monte Carlo methods, then the double randomization technique can be extended over its integration domains. This extension entails sampling a single realization of its corresponding random variables. Our aim is the development of such a path-integral formulation.

The transport of radiance can be described by the stationary form of the monochromatic Radiative Transfer Equation (RTE):

$$\begin{cases} \forall \vec{x} \in \Omega, \forall \vec{u} \in \boldsymbol{S}^2 : \\ \vec{u}.\vec{\nabla} L_\nu(\vec{x}, \vec{u}) = -k_{ext,\nu}(\vec{x}) L_\nu(\vec{x}, \vec{u}) + k_{a,\nu}(\vec{x}) L_\nu^{eq}(T(\vec{x})) \\ \qquad\qquad + k_{s,\nu}(\vec{x}) \int_{4\pi} p_\nu(\vec{u}', \vec{u})\, d\vec{u}'\, L_\nu(\vec{x}, \vec{u}') \\ \forall \vec{y} \in \partial\Omega, \forall \vec{u}_+ \in \boldsymbol{S}_+^2 : \\ L_\nu(\vec{y}, \vec{u}_+) = L_\nu^{\partial\Omega}(\vec{y}, \vec{u}_+) \end{cases} \tag{3}$$

where $\boldsymbol{S}^2$ is the unit sphere, Ω is the geometrical domain (the atmosphere), and $\partial\Omega$ is its boundary (the TOA and the land or oceanic surface), where the monochromatic radiance $L_\nu^{\partial\Omega}$ is known for all locations $\vec{y} \in \partial\Omega$, and all directions $\vec{u}_+$ within the incoming hemisphere $\boldsymbol{S}_+^2$ at position $\vec{y}$. The coefficients $k_{a,\nu}(\vec{x})$, $k_{s,\nu}(\vec{x})$, and $k_{\mathrm{ext},\nu}(\vec{x}) = k_{a,\nu}(\vec{x}) + k_{s,\nu}(\vec{x})$ are the absorption, scattering, and extinction coefficients, respectively. $L_\nu^{eq}(T(\vec{x}))$ is the equilibrium blackbody radiance (following the Planck blackbody radiance function, for temperature $T(\vec{x})$ at location $\vec{x}$), and $p_\nu(\vec{u}', \vec{u})$ is the single scattering phase function, *i.e.*, the probability density that the propagation direction after scattering is $\vec{u}'$ for a given incoming direction $\vec{u}$.

The path-integral formulation corresponding to System (3) is :

$$L_\nu(\vec{x}, \vec{u}) = \int_0^{+\infty} p_{\mathcal{L}}(l) dl \left[\begin{array}{l} \mathcal{H}(\vec{x}' \notin \Omega)\, L_\nu^{\partial\Omega}(\vec{y}, \vec{u}) \\ +\mathcal{H}(\vec{x}' \in \Omega) \left[\begin{array}{l} P_{abs}(\vec{x}')\, L_\nu^{eq}(T(\vec{x}')) \\ +P_{sca}(\vec{x}') \int_{4\pi} p_\nu(\vec{u}', \vec{u})\, d\vec{u}'\, L_\nu(\vec{x}', \vec{u}') \end{array} \right] \end{array} \right], \tag{4}$$

with $p_{\mathcal{L}}(l) = k_{\mathrm{ext},\nu}(\vec{x} - l\vec{u}) e^{-\int_0^l k_{\mathrm{ext},\nu}(\vec{x} - l'\vec{u}) dl'}$ the probability density function for sampling a free path of length l, which provides the next collision position $\vec{x}' = \vec{x} - l\vec{u}$. Eq. (4) can be translated into a backward Monte Carlo algorithm that estimates $L_\nu(\vec{x}, \vec{u})$ as a sum of contributions from emission sources. Each collision position $\vec{x}'$ is either outside the medium ($\mathcal{H}(\vec{x}' \notin \Omega)$), in which case the retained weight is $L_\nu^{\partial\Omega}(\vec{y}, \vec{u})$ (the boundary condition radiance in direction $\vec{u}$ and at position $\vec{y}$, $\vec{y}$ being the position of the first intersection between the $(\vec{x}, \vec{u})$ sightline and the boundary $\partial\Omega$), or $\vec{x}'$ is still in the medium ($\mathcal{H}(\vec{x}' \in \Omega)$) (see Fig. 1). In the latter case, two types of collision events can take place according to probabilities $\mathrm{P_{abs}}(\vec{x}) = k_{a,\nu}(\vec{x})/k_{ext,\nu}(\vec{x})$ and $\mathrm{P_{sca}}(\vec{x}) = k_{s,\nu}(\vec{x})/k_{ext,\nu}(\vec{x})$ for an absorption event or a scattering event, respectively. In the case of an absorption event, the Monte Carlo weight is the blackbody equilibrium radiance $L_\nu^{eq}(T(\vec{x}))$ at the $\vec{x}'$ collision position. Indeed, absorption points in a reverse path correspond to emission points in its corresponding forward path, leveraging the reciprocity of light paths in accordance with the second law of thermodynamics. In the case of a scattering event, the optical trajectory continues in a new propagation direction $\vec{u}'$ sampled according to the phase function $p_\nu(\vec{u}', \vec{u})$; radiance $L_\nu(\vec{x}', \vec{u}')$ for the new position and propagation direction has to be computed. $L_\nu(\vec{x}', \vec{u}')$ has the very same integral formulation as $L_\nu(\vec{x}, \vec{u})$: the path-integral formulation is recursive. The model described does not consider boundary reflection, but its inclusion is straightforward: as a photon reaches the boundary, if it is reflective (*e.g.*, ground reflection), the photon has a probability of being absorbed or reflected back into the medium according to the given reflection model.

The probabilistic model above presents two difficulties. The first one is encountered when sampling the extinction length l, as $L_\nu(\vec{x}, \vec{u})$ depends non-linearly (through an exponential function) on the integral of the heterogeneous extinction coefficient field $k_{ext,\nu}(\vec{x})$. The second one is encountered when sampling the collision type; the absorption coefficient is a sum over millions of molecular transitions: $k_{a,\nu}(\vec{x}) = \sum_{j=1}^{N_t} h_{a,\nu,j}(\vec{x})$ with $h_{a,\nu,j}(\vec{x})$ the contribution of transition of index j to the total absorption coefficient of the medium; this is computationally expensive to estimate. Approximation methods for the calculation of the absorption coefficient field exist and are routinely used in atmospheric radiative transfer, but their model errors can be difficult to quantify. Interestingly, using the null-collision method makes both of these limitations vanish. Not only does introducing fictive colliders homogenize the extinction coefficient field [25] making the sampling of the extinction length l simpler, but it also enables a coupling between the line-by-line spectroscopic model and the radiative transfer model [9,14], where the absorption coefficient is replaced with a transition sampling over the contributing spectral lines. The resulting model now encompasses radiation and spectroscopy in a single path-integral formulation. In terms of model resolution, the model is simulated as a whole in a single Monte Carlo simulation. This particular point becomes more obvious through the algorithmic illustration given in Section 2.3, which is the probabilistic description of the following path-integral formulation, derived in Appendix:

$$L_\nu(\vec{x}, \vec{u}) = \int_0^{+\infty} \hat{p}_{\mathcal{L}}(l) dl \left[\begin{array}{l} \mathcal{H}(\vec{x}' \notin \Omega)\, L_\nu^{\partial\Omega}(\vec{y}, \vec{u}) \\ +\mathcal{H}(\vec{x}' \in \Omega) \left[\begin{array}{l} \hat{P}_s \left\{ \begin{array}{l} P_s(\vec{x}') \int_{4\pi} p_\nu(\vec{u}', \vec{u})\, d\vec{u}'\, L_\nu(\vec{x}', \vec{u}') \\ +(1 - P_s(\vec{x}'))\, L_\nu(\vec{x}', \vec{u}) \end{array} \right\} \\ +(1 - \hat{P}_s) \left(\sum_{j=1}^{N_t} P_J(j, \nu) \left\{ \begin{array}{l} P_{a,\nu,j}(\vec{x}')\, L_\nu^{eq}(T(\vec{x}')) \\ +(1 - P_{a,\nu,j}(\vec{x}'))\, L_\nu(\vec{x}', \vec{u}) \end{array} \right\} \right) \end{array} \right] \end{array} \right] \tag{5}$$

where additional terms are introduced to account for null collisions (see details in Appendix).

This reformulation results in a path-integral where the physics of radiative transfer is nonlinearly coupled to spectroscopy through the introduction of recursive null events. The requirement of pre-computing the absorption coefficient field is shifted to the ability to sample just one transition per each Monte Carlo realization.

Indeed, Eq. (5) can be translated into a Monte Carlo algorithm, for which the procedure for one realization is presented in Algorithm 1.

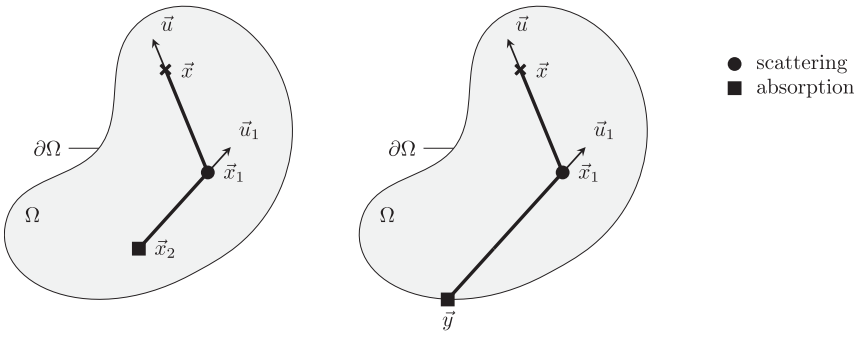

(a) Volume absorption (b) Boundary absorption

Fig. 1. An example of radiance reverse path starting at $\vec{x}$ in direction $\vec{u}$ is shown. It is composed of several scattering events (circle) before finally reaching an absorption event (square) occuring either (a) in the volume Ω, or (b) at the system boundary $\partial\Omega$. Absorption points in a reverse path correspond to emission points in its corresponding forward path, leveraging the reciprocity of light paths in accordance with the second law of thermodynamics.

The optical path associated with each realization can propagate in the medium without knowing the real extinction coefficient field upfront, now needed only locally at each collision location. To sample a collision location, only a number of homogeneous upper bound free parameters are required to define various probabilities: $\hat{k}_{a,\nu}$ is an upper-bound of the absorption coefficient field, $\hat{k}_{s,\nu}$ is an upper-bound of the scattering coefficient field and $\hat{k}_{ext,\nu} = \hat{k}_{a,\nu} + \hat{k}_{s,\nu}$ is an upper-bound of the extinction coefficient field. An upper-bound $\hat{h}_{a,\nu,j}$ of the contribution $h_{a,\nu,j}(\vec{x})$ of transition of index j to the local absorption coefficient must also be defined, so that $\hat{k}_{a,\nu} = \sum_{j=1}^{N_t} \hat{h}_{a,\nu,j}$, where N_t is the total number of transitions. As we will see in next section, we obtain a path-integral of a similar structure for sensitivities, for which we provide a complete description in the algorithmic section.

As far as computational cost is concerned, arbitrarily choosing these uniform upper-bound free parameters does not necessarily ensure an efficient sampling of transitions because absorption spectra are highly varying in frequencies. This can lead to a significant computational cost if chosen too large compared to the true absorption spectra: as $\hat{k}_{\text{ext},\nu}$ increases relative to $k_{\text{ext},\nu}(\vec{x})$, sampled path-lengths l become shorter, and the likelihood of encountering null events increases. Consequently, this necessitates the sampling of a considerable number of consecutive spatial positions to sample a single path. This is where computer scientists' expertise in structuring and processing data comes into play. For an efficient sampling of large spectral data sets, the frequency domain is partitioned inside a hierarchical grid to build a field of upper bounds adapted to the absorption spectra variations. This data structuring makes the computational cost weakly sensitive to the size (number of transitions) and the complexity (shape of absorption spectra) of the spectroscopic database [14]. Given the significant variability of absorption spectra with altitude, mostly due to pressure variations, the spectral hierarchical grids are tabulated as a function of pressure, and algorithmic adjustments are designed such that no alterations are made to the integral formulation represented by Eq. (5).

The next section details the formal developments for obtaining a similar path-integral for sensitivities.

2.2. Estimating global radiative flux sensitivities

The previous section establishes the path-integral Monte Carlo approach for evaluating the global outgoing radiative flux at TOA using an integral reformulation for radiance. In this section, we show how to extend this framework to estimate flux sensitivities, paying specific attention to retaining the benefits associated with the use of the null-collision technique.

Sensitivity with respect to parameter $\ddot{\pi}$ is defined as $\partial_{\ddot{\pi}}\bar{\phi}$ the partial derivative of the flux at TOA. Let s_ν be defined such that $s_\nu(\vec{x},\vec{u},t,\ddot{\pi}) = \partial_{\ddot{\pi}} L_\nu(\vec{x},\vec{u},t,\ddot{\pi})$, then the TOA flux sensitivity is:

$$\begin{aligned}\partial_{\ddot{\pi}}\bar{\phi} = &\int_{\Delta t} p_T(t)dt \int_S p_S(\vec{x})dS(\vec{x}) \int_0^{+\infty} p_N(\nu)d\nu \\ &\times \int_{2\pi} p_U(\vec{u})d\vec{u} \left\{ \frac{\pi s_\nu(\vec{x},\vec{u},t,\ddot{\pi})}{p_N(\nu)} \right\},\end{aligned} \tag{6}$$

which requires a path-integral formulation of s_ν, similar to the path-integral formulation that was required for L_ν in the previous section. In addressing the question of sensitivity estimation using Monte Carlo methods, two different approaches may be considered. The first one consists in differentiating the path-integral formulation of $L_\nu(\vec{x},\vec{u})$ in Eq. (5), and rewriting the resulting integral in order to preserve the same random samplings (and thus, the same algorithmic structure) between the quantity and its derivatives [15]. This is computationally efficient since only one set of paths has to be sampled to estimate all the quantities at once. However, when null-collision algorithms are implemented in combination with acceleration structures to guarantee that only a small fraction of fictive colliders is introduced at any location, [17] has demonstrated that the variance of the sensitivity estimates might be unbounded. This is because the weights that are retained for the sensitivity estimates are inversely proportional to the concentration of fictive colliders, which tends to zero as the acceleration structure is better optimized. [17] proposed a solution to bypass this difficulty, but this requires an additional sampling at each collision event. The second approach, which we choose to explore in the present work, consists in differentiating the radiative transport model of $L_\nu(\vec{x},\vec{u})$ in System (3) to establish a transport model for the sensitivity. This method was originally developed for geometric sensitivities (derivatives with respect to parameters the geometry depends upon [18,19]) ant it will be used hereafter for parametric (non-geometric) sensitivities. This framework enables the physical analysis of sensitivity propagation in the participating medium.

According to the second approach, differentiating System (3) with respect to $\ddot{\pi}$ yields a transport model for the sensitivity that can be expressed using a new transport equation, namely a Sensitivity Transport Equation (STE):

$$\begin{cases} \forall \vec{x} \in \Omega, \forall \vec{u} \in \boldsymbol{S}^2 : \\ \vec{u}.\vec{\nabla}_X s_\nu(\vec{x},\vec{u},\ddot{\pi}) = -k_{ext,\nu}(\vec{x},\ddot{\pi}) s_\nu(\vec{x},\vec{u},\ddot{\pi}) \\ \qquad + k_{a,\nu}(\vec{x},\ddot{\pi})[\frac{\partial_{\ddot{\pi}} k_{a,\nu}(\vec{x},\ddot{\pi})}{k_{a,\nu}(\vec{x},\ddot{\pi})}(L_\nu^{eq}(T(\vec{x})) - L_\nu(\vec{x},\vec{u},\ddot{\pi}))] \\ \qquad + k_{s,\nu}(\vec{x},\ddot{\pi}) \int_{4\pi} p_\nu\left(\vec{u}',\vec{u}\right) d\vec{u}'(s_\nu(\vec{x},\vec{u}',\ddot{\pi}) \\ \qquad + [\frac{\partial_{\ddot{\pi}} k_{s,\nu}(\vec{x},\ddot{\pi})}{k_{s,\nu}(\vec{x},\ddot{\pi})}(L_\nu(\vec{x},\vec{u}',\ddot{\pi}) - L_\nu(\vec{x},\vec{u},\ddot{\pi}))]) \\ \forall \vec{y} \in \partial\Omega, \forall \vec{u}_+ \in \boldsymbol{S}^2_+ : \\ s_\nu(\vec{y},\vec{u}_+) = 0 \end{cases} \tag{7}$$

$$
\begin{aligned}
&s_\nu(\vec{x},\vec{u},\ddot{\pi}) = \int_0^{+\infty} \hat{p}_{\mathcal{L}}(l)dl \\
&\left[\begin{array}{l}
\mathcal{H}\left(\vec{x}' \notin \Omega\right).0 \\
+\mathcal{H}\left(\vec{x}' \in \Omega\right) \\
\quad\left[\begin{array}{l}
\hat{P}_s(\vec{x}')\left\{\begin{array}{l} P_s(\vec{x}')\int_{4\pi} p_\nu\left(\vec{u}',\vec{u}\right)d\vec{u}'\left[s_\nu(\vec{x}',\vec{u}',\ddot{\pi}) + \left[\frac{\partial_{\ddot{\pi}} k_{d,\nu}(\vec{x},\ddot{\pi})}{k_{d,\nu}(\vec{x},\ddot{\pi})}\left(L_\nu(\vec{x}',\vec{u}',\ddot{\pi}) - L_\nu\left(\vec{x}',\vec{u},\ddot{\pi}\right)\right)\right]\right] \\ +\left(1-P_s\left(\vec{x}'\right)\right)\left[s_\nu\left(\vec{x}',\vec{u},\ddot{\pi}\right)\right] \end{array}\right\} \\
+\left(1-\hat{P}_s\left(\vec{x}'\right)\right)\left(\sum_{j=1}^{N_t} P_J(j,\nu)\left\{\begin{array}{l} P_{a,\nu,j}\left(\vec{x}'\right)\left[\frac{\partial_{\ddot{\pi}} h_{a,\nu,j}(\vec{x},\ddot{\pi})}{h_{a,\nu,j}(\vec{x},\ddot{\pi})}\left(L_\nu^{eq}(T(\vec{x}')) - L_\nu(\vec{x}',\vec{u},\ddot{\pi})\right)\right] \\ +\left(1-P_{a,\nu,j}\left(\vec{x}'\right)\right)\left[s_\nu\left(\vec{x}',\vec{u},\ddot{\pi}\right)\right] \end{array}\right\}\right)
\end{array}\right]
\end{array}\right]
\end{aligned}
\tag{8}
$$

Box I.

where the temperature $T(\vec{x})$ and the phase function $p_\nu\left(\vec{u}',\vec{u}\right)$ are independent of the parameter $\ddot{\pi}$.

Comparing STE (Eq. (7)) with RTE (Eq. (3)), we see that the structure for transport of sensitivity is very similar to that of radiance, which translates into the same sampling procedure between the two quantities. The difference only regards the sources via absorption and scattering.

At this point, the STE can be solved using any model for the absorption and scattering coefficients fields $k_{a,\nu}(\vec{x},\ddot{\pi})$ and $k_{s,\nu}(\vec{x},\ddot{\pi})$. However, it is possible to establish a sensitivity model that couples line-by-line spectroscopy and radiative transfer, following the same formal developments (in Appendix) used for the construction of the multiphysics model of radiance. Doing so, we obtain a path-integral formulation for sensitivity similar to the path-integral formulation for radiance in Eq. (5) is given as Eq. (8) in Box I.

The resulting path-integral formulation can correspond to multiple Monte Carlo algorithmic interpretations. We will now elaborate on the specificities of our simulation choices.

2.3. From path-integral formulation to Monte Carlo algorithm

We can read in our sensitivity path-integral formulation (Eq. (8)) a coupling to two other path-integrals corresponding to two distinct physics. The first coupling is to the line-by-line spectroscopic model through $P_{a,\nu,j}$, governing real or null transitions. The second coupling is to the radiance model L_ν, which appears in the weights of sensitivity Monte Carlo realizations. We refer to these through *coupling* because the sensitivity path-integral is designed in a way that a single Monte Carlo iteration walks across different physics by sampling their associated random variables — here, radiance and absorption coefficient — without requiring their explicit calculation. Instead, only one realization of each corresponding random variable is sampled.

This becomes manifest in the statistical procedure for sampling a single Monte Carlo weight presented in Algorithm 2, which is a strict translation of the sensitivity path-integral formulation presented in Eq. (8). The complete Monte Carlo for sensitivity estimation entails N averaged realizations, each sampled as follows:

- Initialization: start an optical path at position $\vec{x}$, in direction $-\vec{u}$.
- Sampling path length: sample path length l according to $\hat{p}_{\mathcal{L}}(l) = \hat{k}_{ext,\nu}\exp\left(-\hat{k}_{ext,\nu}l\right)$ over $[0,+\infty)$.
- Update position : $\vec{x}' = \vec{x} - l\vec{u}$.
- Boundary check: check whether $\vec{x}'$ is outside or inside Ω.
  - If outside, the weight is the boundary condition (here it is null because the boundary conditions in the model of L was set independent of the parameter), and the realization stops.
  - If inside, proceed to collision branch determination at $\vec{x}'$.
- Collision branch determination: determine the collision type by sampling between the *scattering branch* and the *absorption branch* with probabilities $\hat{P}_s(\vec{x}')$ and $\hat{P}_a(\vec{x}') = 1 - \hat{P}_s(\vec{x}')$, respectively.
- If the "scattering branch" is selected: determine whether it is a real or a null scattering event with probabilities $P_s(\vec{x}')$ and $1 - P_s(\vec{x}')$, respectively.
  - If real scattering event: the new propagation direction $\vec{u}'$ has to be sampled over 4π sr according to the $p(\vec{u}',\vec{u})$ probability density function. Then we evaluate $s_\nu(\vec{x}',\vec{u}',\ddot{\pi})$ by recursing on Algorithm 2; we also evaluate $L_\nu(\vec{x}',\vec{u}',\ddot{\pi})$ and $L_\nu\left(\vec{x}',\vec{u},\ddot{\pi}\right)$ using Algorithm 1 via double randomization, meaning we estimate one Monte Carlo realization of Algorithm 1 at position $\vec{x}'$ and direction $\vec{u}'$ and at $\vec{x}'$ and direction $\vec{u}$, respectively. The Monte Carlo weight we retain is then $s_\nu(\vec{x}',\vec{u}',\ddot{\pi}) + \left[\frac{\partial_{\ddot{\pi}} k_{d,\nu}(\vec{x},\ddot{\pi})}{k_{d,\nu}(\vec{x},\ddot{\pi})}\left(L_\nu(\vec{x}',\vec{u}',\ddot{\pi}) - L_\nu\left(\vec{x}',\vec{u},\ddot{\pi}\right)\right)\right]$, and additional data has to be known at this point: the value of $\partial_{\ddot{\pi}} k_{d,\nu}(\vec{x},\ddot{\pi})$.
  - If null scattering event: recurse on Algorithm 2 at the new position $\vec{x}'$ but in the same direction $\vec{u}$.
- If the "absorption branch" is selected: sample a transition according to the $P_J(j,\nu) = \frac{\hat{h}_{a,\nu,j}}{\hat{k}_{a,\nu}}$, $j \in [1,N_t]$ probability set. Then determine whether it is a real or a null transition event with probabilities $P_{a,\nu,j}(\vec{x}') = \frac{h_{a,\nu,j}(\vec{x})}{\hat{h}_{a,\nu,j}}$ and $1 - P_{a,\nu,j}(\vec{x}') = \frac{\hat{h}_{a,\nu,j} - h_{a,\nu,j}(\vec{x})}{\hat{h}_{a,\nu,j}}$, respectively.
  - If real transition event: the weight $\frac{\partial_{\ddot{\pi}} h_{a,\nu,j}(\vec{x},\ddot{\pi})}{h_{a,\nu,j}(\vec{x},\ddot{\pi})}\left(L_\nu^{eq}(T(\vec{x}')) - L_\nu(\vec{x}',\vec{u},\ddot{\pi})\right)$ is retained and the realization stops. Two additional quantities need to be evaluated: the value of $\partial_{\ddot{\pi}} h_{a,\nu,j}(\vec{x},\ddot{\pi})$ and $L_\nu(\vec{x}',\vec{u},\ddot{\pi})$. The latter is evaluated by a single realization of the corresponding radiance random variable, relying on double randomization.
  - If null transition event: recurse on Algorithm 2 at the new position $\vec{x}'$ but in the same direction $\vec{u}$.

This algorithmic translation is facilitated by leveraging a mathematical statistical property encapsulated in Box 1, initially introduced in the work [26]. In our model, this property is particularly relevant, as sensitivity, akin to radiance, shares a structural similarity with g in Box 1, which arises from specific formal development choices made during the construction of Eq. (8) for sensitivity (and Eq. (5) for radiance). To draw a parallel, sampling a single realization of X to determine the Bernoulli parameter $P = \frac{X}{\hat{x}}$ in the Box — instead of computing its expectation —, is the theoretical justification in our model for sampling a single transition to determine the absorption probability — instead of pre-computing the absorption coefficient — [14]. Subsequently, a Bernoulli trial follows to determine whether it corresponds to a real or null absorption, thus retaining the corresponding sensitivity weight (or radiance weight).

Fig. 2 illustrates a sensitivity path in pink, consisting of a sequence of consecutive collision events. The physics coupling is visually conveyed through path branches, with the rainbow representing the spectroscopy and yellow representing the radiance model. The distinct

Algorithm 1 Radiance realization $L_\nu(\vec{x},\vec{u},\lambda)$

Input: a position $\vec{x}$, a direction $\vec{u}$, a parameter λ
Output: a Monte Carlo radiance weight ω
function RadianceRealization($\vec{x}$, $\vec{u}$, λ)
  Sample a length to the next collision position l according to $\hat{p}_{\mathcal{L}}(l)$
  Compute the next collision position $\vec{x}' \leftarrow \vec{x} - l\vec{u}$
  if $\vec{x}' \notin \Omega$ **then**
    Compute position $\vec{y}$ of intersection between $(\vec{x},-\vec{u})$ ray and boundary $\partial\Omega$
    $\omega \leftarrow L_\nu^{\partial\Omega}(\vec{y},\vec{u})$
  else
    Sample a uniform random variable $r \in [0,1]$
    if $r < \hat{P}_s(\vec{x}')$ **then** /* *scattering* */
      Sample a uniform random variable $r \in [0,1]$
      if $r < P_s(\vec{x}')$ **then** /* *real-scattering event* */
        Sample scattering direction $\vec{u}'$ according to phase function $p(\vec{u}',\vec{u})$
        $\omega \leftarrow$ RadianceRealization($\vec{x}'$, $\vec{u}'$, λ) ▷ ***Recurse*** Algo. 1
      else /* *null-scattering event* */
        $\omega \leftarrow$ RadianceRealization($\vec{x}'$, $\vec{u}$, λ) ▷ ***Recurse*** Algo. 1
      end if
    else /* *absorption* */
      Sample a transition j according to $P_J(j,\nu)$
      Sample a uniform random variable $r \in [0,1]$
      if $r < P_{a,j}(\vec{x}')$ **then** /* *real-transition event* */
        $\omega \leftarrow L_\nu^{eq}(T(\vec{x}'))$
      else /* *null-transition event* */
        $\omega \leftarrow$ RadianceRealization($\vec{x}'$, $\vec{u}$, λ) ▷ ***Recurse*** Algo. 1
      end if
    end if
  end if
  return ω
end function

Algorithm 2 Sensitivity realization $s_\nu(\vec{x},\vec{u},\lambda)$

Input: a position $\vec{x}$, a direction $\vec{u}$, a parameter λ
Output: a Monte Carlo sensitivity weight ω
function SensitivityRealization($\vec{x}$, $\vec{u}$, λ)
  Sample a length to the next collision position l according to $\hat{p}_{\mathcal{L}}(l)$
  Compute the next collision position $\vec{x}' \leftarrow \vec{x} - l\vec{u}$
  if $\vec{x}' \notin \Omega$ **then**
    $\omega \leftarrow 0$
  else
    Sample a uniform random variable $r \in [0,1]$
    if $r < \hat{P}_s(\vec{x}')$ **then** /* *scattering* */
      Sample a uniform random variable $r \in [0,1]$
      if $r < P_s(\vec{x}')$ **then** /* *real-scattering event* */
        Sample scattering direction $\vec{u}'$ according to phase function $p(\vec{u}',\vec{u})$
        $L_\nu(\vec{x}',\vec{u}',\lambda) \leftarrow$ RadianceRealization($\vec{x}'$, $\vec{u}'$, λ) ▷ Algo. 1
        $L_\nu(\vec{x}',\vec{u},\lambda) \leftarrow$ RadianceRealization($\vec{x}'$, $\vec{u}$, λ) ▷ Algo. 1
        $s_\nu(\vec{x}',\vec{u}',\lambda) \leftarrow$ SensitivityRealization($\vec{x}'$, $\vec{u}'$, λ) ▷ ***Recurse*** Algo. 2
        $\omega \leftarrow s_\nu(\vec{x}',\vec{u}',\lambda) + \frac{\partial_{\tilde{\lambda}} k_{d,\nu}(\vec{x},\tilde{\lambda})}{k_{d,\nu}(\vec{x},\lambda)}(L_\nu(\vec{x}',\vec{u}',\lambda) - L_\nu(\vec{x}',\vec{u},\lambda))$
      else /* *null-scattering event* */
        $\omega \leftarrow$ SensitivityRealization($\vec{x}'$, $\vec{u}$, λ) ▷ ***Recurse*** Algo. 2
      end if
    else /* *absorption* */
      Sample a transition j according to $P_J(j,\nu)$
      Sample a uniform random variable $r \in [0,1]$
      if $r < P_{a,j}(\vec{x}')$ **then** /* *real-transition event* */
        Compute equilibrium blackbody radiance $L_\nu^{eq}(T(\vec{x}'))$
        $L_\nu(\vec{x}',\vec{u},\lambda) \leftarrow$ RadianceRealization($\vec{x}'$, $\vec{u}$, λ) ▷ Algo. 1
        $\omega \leftarrow \frac{\partial_{\tilde{\lambda}} h_{a,\nu,j}(\vec{x},\tilde{\lambda})}{h_{a,\nu,j}(\vec{x},\lambda)}(L_\nu^{eq}(T(\vec{x}')) - L_\nu(\vec{x}',\vec{u},\lambda))$
      else /* *null-transition event* */
        $\omega \leftarrow$ SensitivityRealization($\vec{x}'$, $\vec{u}$, λ) ▷ ***Recurse*** Algo. 2
      end if
    end if
  end if
  return ω
end function

nature of these two physics branches is particularly noteworthy. The spectroscopic rainbow branch contributes to constructing the sensitivity path, determining whether it continues beyond a collision site in the absorption branch. In contrast, each yellow radiance branch samples information that will contribute to the sensitivity Monte Carlo weight but not to the construction of the sensitivity path. This difference in the two coupling statuses is grounded in the differential form of the STE. On the one hand, the sensitivity transport model exhibits a non-linear dependency on the absorption coefficient through Beer's exponential, which is bypassed using null collisions. On the other hand, the radiance appears as a volumetric source term in the STE, hence the linearity of the radiance-sensitivity coupling.

1- A mathematical property for our statistical framework

This box demonstrates that if g is the expectation of a Bernoulli random variable (with possible outcomes $\mathbb{E}(Y)$ and $\mathbb{E}(Z)$) where the probability is itself the expectation of a random variable $\frac{X}{\hat{x}}$ whose domain is the interval $[0,1]$, then the expectation of W is an unbiased estimator for g, where a single realization of $\frac{X}{\hat{x}}$ is sampled for each realization of W.

Property: Let g be a function of the expectancy of random variables X, Y, and Z, defined by the following structure:

$$g = \frac{\mathbb{E}(X)}{\hat{x}} \cdot \mathbb{E}(Y) + \left[1 - \frac{\mathbb{E}(X)}{\hat{x}}\right] \cdot \mathbb{E}(Z)$$

where $\hat{x}$ is an upper bound for *all* realizations x of X, and the pairs of variables (X,Y) and (X,Z) are statistically independent.
Then g is the expectation of random variable W:

$$g = \mathbb{E}(W)$$

such that:

$$W = B\left(\frac{X}{\hat{x}}\right) \cdot Y + \left[1 - B\left(\frac{X}{\hat{x}}\right)\right] \cdot Z$$

where $B\left(\frac{X}{\hat{x}}\right)$ is the Bernoulli variable of parameter the random variable $P = \frac{X}{\hat{x}}$.

Demonstration: By definition of g, we have:

$$g = \frac{\int_{D_X} x p_X(x)\,dx}{\hat{x}} \cdot \int_{D_Y} y p_Y(y)\,dy + \left[1 - \frac{\int_{D_X} x p_X(x)\,dx}{\hat{x}}\right] \cdot \int_{D_Z} z p_Z(z)\,dz$$

with p_X, p_Y and p_Z the probability density functions associated to random variables X, Y and Z, respectively.
It can be reformulated as:

$$g = \int_{D_X} p_X(x)\,dx \left(\frac{x}{\hat{x}} \cdot \int_{D_Y} y p_Y(y)\,dy + \left[1 - \frac{x}{\hat{x}}\right] \cdot \int_{D_Z} z p_Z(z)\,dz\right)$$

3. Results and discussions

3.1. Results

In the following, we use as the inputs of our spectro-radiative model, atmospheric state outputs from a simulation performed with the IPSL General Circulation Model 3.1. [27] (vertical profiles of pressure, temperature, and molecular species concentration). The IPSL climate model simulation was performed on a 144 × 143 longitude-latitude grid using 79 vertical levels. We use 3-hourly outputs of a 10-year simulation, which amounts to a total of $144 \times 143 \times 10 \times 365 \times 8 \approx 600$ million columns. The computations are performed in clear sky conditions considering four greenhouse gases (H_2O, CO_2, O_3, and CH_4), and using a line-by-line spectroscopic model with parameters sourced from the HITRAN database [28]. The Lorentz function describes the profile lineshapes, truncated at 25 cm^{-1} for H_2O, O_3, CH_4, and 50 cm^{-1} for CO_2. Analytical Lorentz profiles are used here, but the methodology extends to Voigt profiles with no further conceptual challenges, where the only additional requirement is data on the corresponding numerical derivatives of the profiles. Also, the water vapor continuum is not

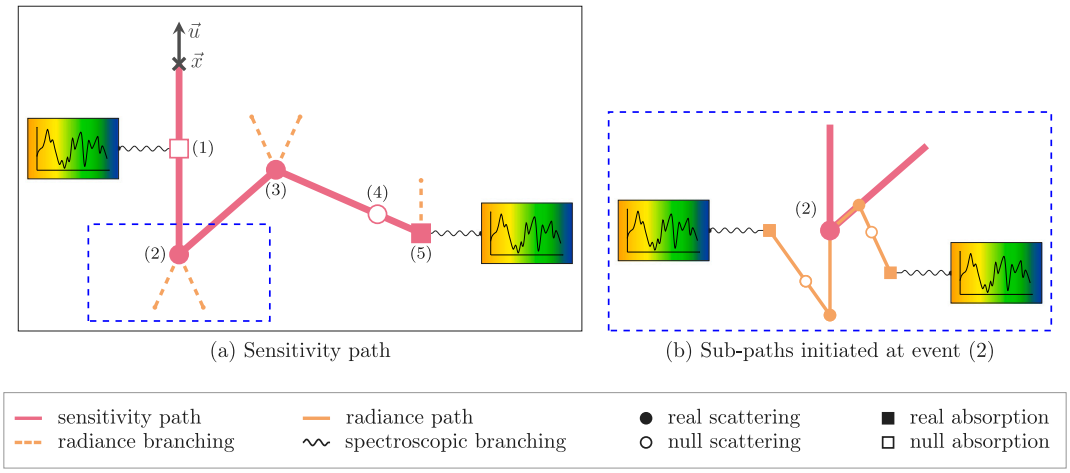

(a) Sensitivity path (b) Sub-paths initiated at event (2)

Fig. 2. On the left side, we depict an instance of the sensitivity reverse path in pink, starting at point $\vec{x}$ in direction $\vec{u}$. The nodes along the path represent real (filled) or null (empty) events of two distinct types: scattering (circle) or absorption (square). Along the sensitivity path, branching sub-paths emerge at these nodes based on their type, invoking either spectroscopic sub-paths in rainbow, radiance sub-paths in yellow, or both. This specific sensitivity path consists of five events. (1) is an absorption event that was randomly determined as being null after sampling a transition where a rainbow spectroscopic sub-path was launched to determine the event type; (2) is a real scattering event; in this case, two yellow radiance sub-paths were launched as a contribution to the path weight; (3) is a similar real scattering event; (4) is a null scattering event without sub-path branchings and (5) is an absorption event that was randomly determined as being real after sampling a transition where a rainbow spectroscopic sub-path was launched to determine the event type, and in this case, a yellow radiance sub-path was launched as a contribution to the path weight. The right panel displays a zoom on scattering event (2): radiance paths are similar to those of sensitivity but only contain rainbow spectroscopic branchings for path construction.

accounted for in the present simulations, and its inclusion would similarly present no further conceptual difficulties.

The theoretical developments are applicable to any parameter of interest in the spectro-radiative model. Here, we focus on the radiative forcings resulting from a fractional change in greenhouse gas concentration. Therefore, we define a sensitivity parameter $\ddot{\pi}$ that acts on the concentration fields and consequently on radiative fluxes through molecular transitions $h_{a,\nu,j}(\vec{x},\ddot{\pi})$ as a multiplier factor of the reference molar fraction of gas, *i.e.*, $x_{\text{gas}} = \ddot{\pi}\times x_{\text{gas, ref}}$. The initial concentration of carbon dioxide is set to the pre-industrial era value $x_{\text{CO}_2,\text{ref}} = 280$ ppm. Each spectral line of index j is modeled as the product of molecular density n, line intensity S_j, and line profile $f_{\nu,j}$. The dependence on parameter $\ddot{\pi}$ intervenes in molecular density $n(\vec{x},\ddot{\pi})$ and line profile $f_{\nu,j}(\vec{x},t,\ddot{\pi})$. The derivative of a spectral line $h_{a,\nu,j}(\vec{x},\ddot{\pi})$ with respect to $\ddot{\pi}$ is then given by:

$$\partial_{\ddot{\pi}} h_{a,\nu,j}(\vec{x},\ddot{\pi}) = \partial_{\ddot{\pi}}\left[\ddot{\pi} n(\vec{x}) S_j(\vec{x}) \frac{\ddot{\pi}\gamma_j}{(\ddot{\pi}\gamma_j)^2 + (\nu - \nu_{0,j})^2}\right] \tag{9}$$

where γ_j and $\nu_{0,j}$ represent, respectively, the linewidth and the central frequency associated with spectral line j.

Using Algorithm 1, we obtain the integrated TOA mean flux $\bar{\phi}$ depicted in Fig. 3(a), 3(c), and 3(e). Using Algorithm 2, we obtain the integrated TOA mean flux sensitivity $\partial_{\ddot{\pi}}\bar{\phi}$ shown in Fig. 3(b), 3(d), and 3(f), with respect to parameter values $\ddot{\pi}$ affecting CO_2, H_2O, and CH_4. The figures illustrate these quantities as a function of parameter values $\ddot{\pi}$. Each point corresponds to an independent estimation, conducted globally over a month and spanning the thermal infrared range $[100; 2500]$ cm^{-1} with $N = 640\,000$ Monte Carlo realizations each.

Fig. 4 represents the dependence of computational time required for achieving a 1% relative error on sensitivity estimates (on a personal computer with 12 CPUs), as a function of the widening in the spectral, spatial and temporal integration domains.

3.2. Discussions

In discussing the results, we focus on three key aspects: (i) in Section 3.2.1, we address the advantages of estimating sensitivity through path-integral Monte Carlo simulations compared to finite differences methods; (ii) in Section 3.2.2, we analyze the computation times as the integration domains are widened; and (iii) in Section 3.2.3, we validate our methods by comparing our results to a well-established functional dependency of the global TOA radiative flux upon fraction change in carbon dioxide concentrations.

3.2.1. *On sensitivity estimation*

For a given gas and across all values of $\ddot{\pi}$, the perturbation of $\ddot{\pi}$ we considered in the results corresponds to injecting the same infinitesimal amount $\mathrm{d}x_{\text{gas}} = x_{\text{gas, ref}} \times \mathrm{d}\ddot{\pi}$ of gas into the atmosphere. The resulting sensitivity $\partial_{\ddot{\pi}}\bar{\phi}$ is the variation in the global outgoing flux at TOA. As anticipated, the negative sensitivities reflect the expected decrease in outgoing flux with an increase in greenhouse gas concentration, in line with the greenhouse effect. Comparing forcings due to different gases, a higher forcing from a gas corresponds to a greater expected impact when increasing its concentration, consistent with the obtained sensitivities; water vapor exhibits larger sensitivities than carbon dioxide and methane, given its greater abundance (see Fig. 3(d) and 3(f)).

For water vapor and carbon dioxide, the finite differences resulting from two distinct Monte Carlo estimations of the flux provide reasonably accurate approximations of the estimated path-integral sensitivities. However, for methane, where variations in mean flux are small (see Fig. 3(e)), finite differences exhibit large fluctuations, contrasting with the more stable path-integral sensitivity estimates (see Fig. 3(f)). Moreover, Monte Carlo estimation provides unbiased sensitivities along with their statistical uncertainty, whereas the uncertainty of finite differences comes from the uncertainties of flux estimation mixed with the uncertainty due to the discretization choice, the latter being impossible to quantify in practice. Moreover, if we keep the same number of realizations, the finer the discretization parameter h, the more relevant the finite differences approximation becomes, but the larger the associated Monte Carlo variance, which increase proportionally to $1/h^2$:

$$\begin{aligned}\partial_{\ddot{\pi}}\bar{\phi}(\ddot{\pi}) &\approx \frac{\bar{\phi}(\ddot{\pi}+h) - \bar{\phi}(\ddot{\pi}-h)}{2h}\\ \sigma^2\left[\partial_{\ddot{\pi}}\bar{\phi}(\ddot{\pi})\right] &\approx \frac{1}{4h^2}\left\{\sigma^2[\bar{\phi}(\ddot{\pi}+h)] + \sigma^2[\bar{\phi}(\ddot{\pi}-h)]\right\}\end{aligned} \tag{10}$$

The advantage of the approach becomes clear: instead of substantially increasing the number of Monte Carlo realizations on flux estimates in order to obtain reliable estimations through finite differences, we propose to use unbiased path-integral formulations for direct sensitivity estimations.

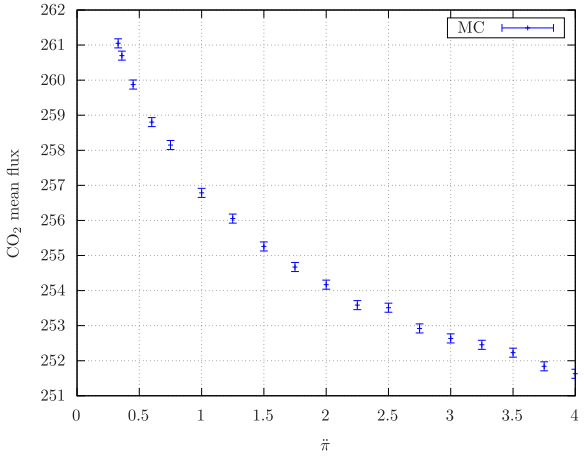

(a) Variation of $\bar{\phi}$ as a function of fraction change in x_{CO_2}.

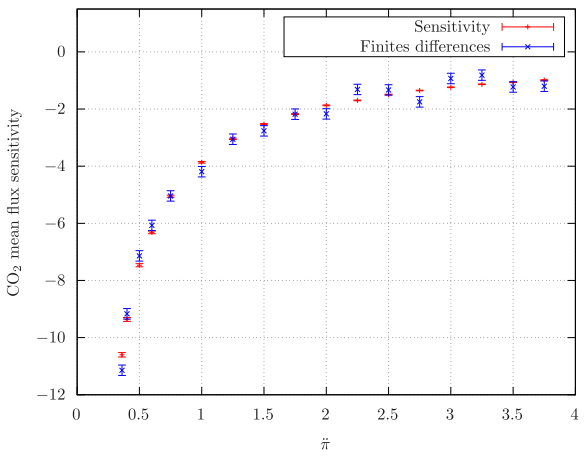

(b) Variation of $\partial_{\ddot{\pi}}\bar{\phi}$ as a function of fraction change in x_{CO_2}.

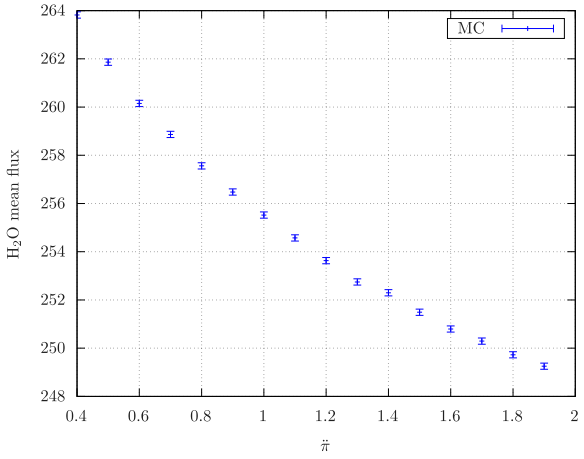

(c) Variation of $\bar{\phi}$ as a function of fraction change in x_{H_2O}.

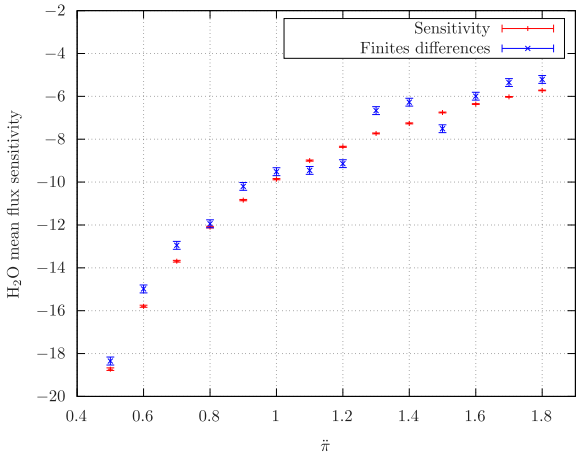

(d) Variation of $\partial_{\ddot{\pi}}\bar{\phi}$ as a function of fraction change in x_{H_2O}.

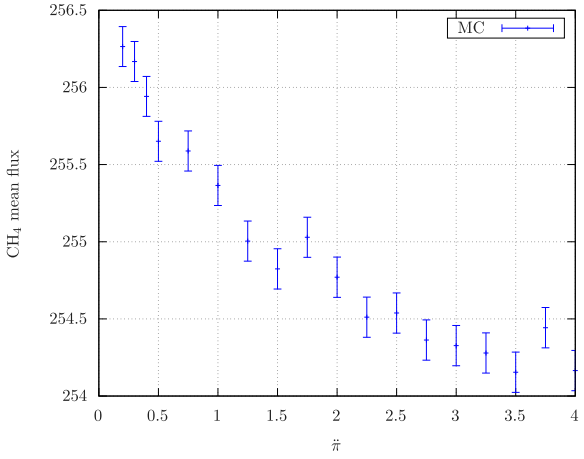

(e) Variation of $\bar{\phi}$ as a function of fraction change in x_{CH_4}.

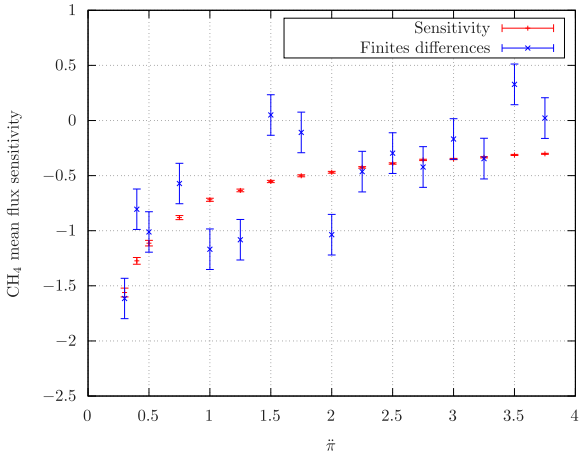

(f) Variation of $\partial_{\ddot{\pi}}\bar{\phi}$ as a function of fraction change in x_{CH_4}.

Fig. 3. Mean flux $\bar{\phi}$ and its sensitivities $\partial_{\ddot{\pi}}\bar{\phi}$ associated to a change in the fraction of gas concentration $\ddot{\pi}$ are displayed for three gases: CO_2 (Fig. 3(a) and 3(b)), H_2O (Fig. 3(c) and 3(d)), and CH_4 (Fig. 3(e) and 3(f)). Sensitivity estimates are obtained using Algorithm 2, whereas finite difference estimates are based on the difference between two standard Monte Carlo flux estimates obtained for different values of $\ddot{\pi}$ using Algorithm 1. Error bars: 68% CI (using 1σ).

3.2.2. On the computation time and Monte Carlo standard deviation

Fig. 4 illustrates how $t_{1\%}$, the computational time required to achieve a 1% error on $\partial_{\ddot{\pi}}\bar{\phi}$ estimates for carbon dioxide, depends on the widening of the respective integration domains, on a personal computer with 12 CPUs. In the first plot, we consider a single atmospheric column and a specific date, for which the quantity $t_{1\%}$ is represented as a function of spectral integration over a band of increasing width, ranging from 10 cm^{-1} (marked by the first red dot) to 2 400 cm^{-1} (the entire infrared range shown in the last red dot). Moving to the middle and the last plots, $\partial_{\ddot{\pi}}\bar{\phi}$ is additionally integrated over spatial and time domains

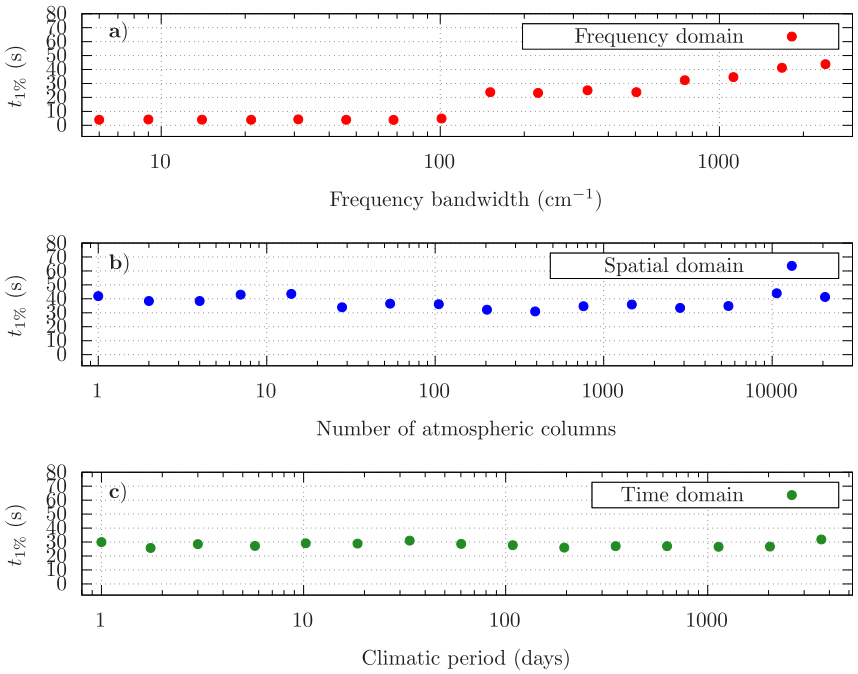

Fig. 4. Computation time required to estimate sensitivity of an outgoing radiative flux with respect to fraction change in CO_2 concentration field, estimated at a 1% relative error using 1σ, showing only a slight dependency to the frequency bandwidth (first plot), spatial (second plot) and temporal (third plot) domains widening.

of increasing size, from 1 to 20 592 atmospheric columns and over a time period ranging from one day up to ten years, respectively.

First of all, on spectral integration, we observe from the first plot that computation time slightly increases with domain widening. Looking at the sensitivity path-integral in Eq. (8), during the Monte Carlo sampling of carbon dioxide sensitivity, the retained weight values depend on the derivative of the spectral line for a given parameter $\ddot{\pi}$, and thus on which concentration field it acts upon. The initial red dot on the graph corresponds to frequency integration within the 15 µm CO_2 band (approximately from 600 cm^{-1} to 700 cm^{-1} on Fig. 5). Subsequent red points, up to an integration width of 100 cm^{-1}, remain within the same band. Consequently, computational time remains insensitive in this band. This comes as no surprise as CO_2 contribution relative to other molecules is dominant in this band. However, as the integration domain is enlarged, within spectral intervals devoid of CO_2 contribution, the sensitivity weight consistently tends to zero, due to contributions from other molecular species, such as H_2O, O_3, and CH_4, that become dominant. Consequently, higher proportions of sensitivity weights yield null values as absorption becomes frequently attributed to these alternative molecules. This introduces a source of greater variance, necessitating additional Monte Carlo realizations to mitigate it, resulting in the observed increase in $t_{1\%}$. While Monte Carlo variance reduction techniques, such as importance sampling — in our case, to minimize the sampling of absorptions by H_2O, O_3, and CH_4— offer a prospective avenue for strategically sampling sensitivity weights, it falls beyond the scope of the present work.

Concerning the second and third plots, we note that expanding both the spatial and temporal integration domains has a negligible impact on computational time, maintaining consistent performance within a range of a few tens of seconds. Now, upon closer examination, the transition from the second to the third plot, corresponding to the introduction of the additional integration domain over time, leads to a 25% reduction in computational cost (from ∼ 40 s to ∼ 30 s), which can be surprising. As a matter of fact, among the time points considered, there might be more or less favorable cases in terms of variance, and hence, convergence. If the expansion of a certain integration dimension is anticipated to decrease the *proportion* of cases with the highest variance, then maintaining the same level of statistical precision would require reduced computational costs as the expansion takes place. Therefore, an additional integration domain in Monte Carlo simulations may sometimes reduce computational costs, *e.g.* [29], as it seems to be the case here. This aspect remains open for further analysis in future research.

We observe that in a general sense, *for the same level of data resolution*, estimating sensitivity for a given date and position on the entire frequency domain (last red point) is nearly as costly as integrating over the entire thermal infrared band, over the entire Earth, and over ten years (last green point).

3.2.3. *From carbon dioxide sensitivity to its radiative forcing estimation*

The central focus of this paper has revolved around developing spectro-radiative path-integrals for sensitivities, designed for unbiased Monte Carlo simulations. The approach avoids approximation schemes at both levels of physics modeling and simulation, thereby providing, for the first time, a method for reference estimations for sensitivities of radiative integrated fluxes to spectroscopic parameters. As a final prospect, we use the approach in the context of radiative forcings, on our simplified configuration.

It is well-known in climate science that the radiative forcing from carbon dioxide is approximately logarithmic in its concentration [30], a property further explained in recent studies [31]. Indeed, the sensitivity to a logarithmic change in its fraction concentration field can be approximated by a constant a:

$$\frac{\mathrm{d}\bar{\phi}}{\mathrm{d}\ln\left(\frac{x_{\mathrm{gas}}}{x_{\mathrm{gas,ref}}}\right)} = a \tag{11}$$

This translates in our model as a functional form independent of the initial concentration field $x_{\mathrm{gas,ref}}$, as it can be reformulated solely as a function of the parameter $\ddot{\pi}$, representing the fractional change:

$$\frac{\mathrm{d}\bar{\phi}}{\mathrm{d}\ln\left(\frac{x_{\mathrm{gas}}}{x_{\mathrm{gas,ref}}}\right)} = \frac{\mathrm{d}\bar{\phi}}{\mathrm{d}\ln(\ddot{\pi})} = \frac{\mathrm{d}\bar{\phi}}{\mathrm{d}\ddot{\pi}} \cdot \ddot{\pi} \tag{12}$$

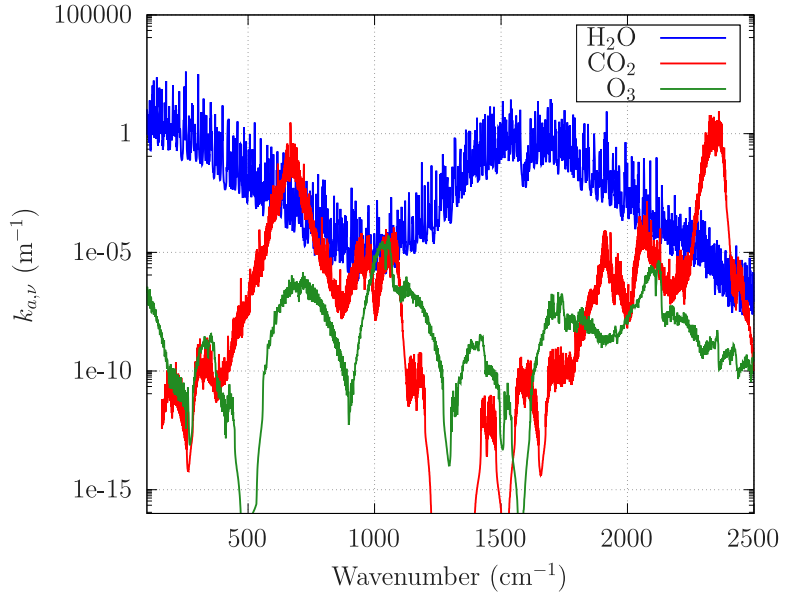

Fig. 5. Spectra across the thermal infrared range [100 cm^{-1}; 2500 cm^{-1}] for the most absorbing molecules in this frequency domain [28].

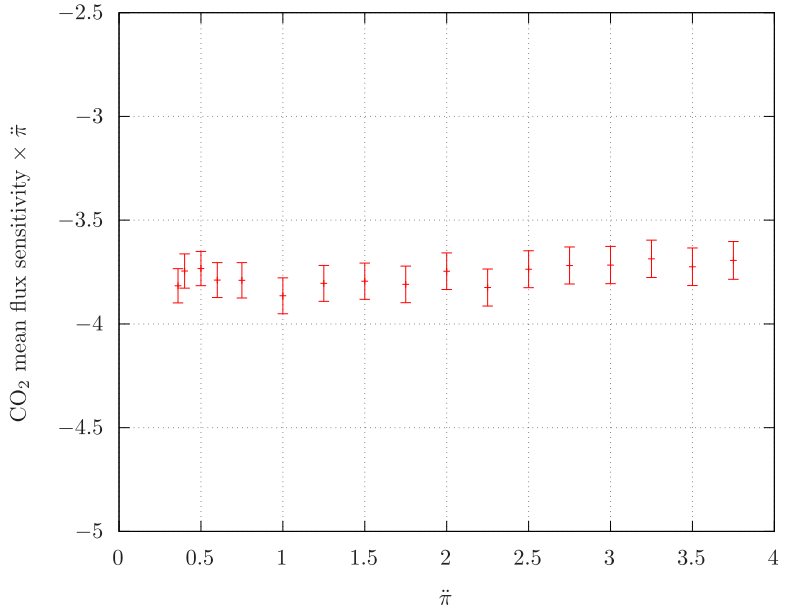

Fig. 6. Evolution of $\partial_{\ddot{\pi}}\bar{\phi}$ (CO_2 sensitivity) multiplied by parameter $\ddot{\pi}$ as a function of $\ddot{\pi}$. Error bars: 99% CI (using 3σ).

This functional dependence property of CO_2 can now be illustrated using our Monte Carlo simulations by plotting the estimated sensitivity $\partial_{\ddot{\pi}}\bar{\phi}$, multiplied by $\ddot{\pi}$, against $\ddot{\pi}$. As illustrated in Fig. 6, this results indeed in a constant value. Our path-integral sensitivity approach thus provides an independent simulation of this logarithmic dependence.

As a matter of fact, we can also note that a single value of our sensitivity estimations — let us choose $a = -3.86 \pm 0.06$ found for $\ddot{\pi} = 1$, taken as a reference case — enables the estimation of carbon dioxide radiative forcing for any fractional change in its concentration, given its functional dependency property. For instance, the radiative forcing for a doubling of the carbon dioxide concentration field yields $\Delta\bar{\phi} = a \ln(2) = -2.68 \pm 0.06$ W/m^2, consistent with recent literature estimates [20].

4. Conclusions

The intention of the present work was to develop a Monte Carlo approach that provides unbiased and efficient spectro-radiative sensitivity estimates. Notably, the approach is employed in the context of estimating atmospheric radiative forcings within a clear-sky simplified climate framework.

By applying Monte Carlo within this framework, we illustrate a well-known property in climate science—the logarithmic tendency of radiative forcing from carbon dioxide in relation to its concentration.

The methodology is constructed to remain unbiased at both levels of physics modeling and simulation. On the theoretical level, sensitivity is regarded as a transported quantity with its own propagation physics,

for which a path-integral solution is constructed. In this regard, we build upon recent advances in coupling the radiative transfer model to the spectroscopic model in a non-linear manner through the absorption coefficient, which disappears from the resulting model. After the formal developments are elaborated, the corresponding probabilistic description is provided in algorithmic form.

The simulation results presented in the preceding section illustrate the practicality of the approach within high-dimensional configurations, such as a climate one. In this context, the estimated quantity is integrated across the entire thermal infrared band, over the whole globe, and over a climate period of ten years. Thanks to advanced computer graphics techniques, achieving a precision of 1 percent on sensitivity estimates required only a few tens of seconds of computation time on a personal computer with 12 CPUs. The high-performance computing times make possible the extensive use of this calculation code for conducting various analyses on the mechanisms of radiative forcings, where it can otherwise be considered too resource-intensive.

Scalability is demonstrated, and while minor convergence variabilities arise depending on the widening of integration domains to maintain the same confidence interval, standard optimization avenues in Monte Carlo practice exist and can be considered based on specific needs. However, these optimizations were deliberately excluded from the present work.

5. Data, materials, and software

Code data is available at (https://gitlab.com/yanissnp/RadForcE).

CRediT authorship contribution statement

Nada Mourtaday: Writing – review & editing, Writing – original draft, Validation, Software, Supervision, Methodology, Investigation, Formal analysis, Conceptualization. **Mégane Bati:** Writing – review & editing, Writing – original draft, Visualization, Software, Conceptualization. **Stéphane Blanco:** Writing – review & editing, Writing – original draft, Methodology, Conceptualization. **Jean-Louis Dufresne:** Writing – review & editing, Writing – original draft, Funding acquisition, Formal analysis, Conceptualization. **Mouna El Hafi:** Writing – review & editing, Writing – original draft, Conceptualization. **Vincent Eymet:** Writing – review & editing, Writing – original draft, Conceptualization. **Vincent Forest:** Software, Conceptualization. **Richard Fournier:** Writing – review & editing, Writing – original draft, Methodology, Conceptualization. **Jacques Gautrais:** Writing – review & editing, Writing – original draft, Conceptualization. **Paule Lapeyre:** Writing – original draft, Methodology, Conceptualization. **Yaniss Nyffenegger-Péré:** Writing – review & editing, Writing – original draft, Validation, Software, Methodology, Investigation, Formal analysis, Conceptualization. **Najda Villefranque:** Writing – review & editing, Writing – original draft, Conceptualization.

Declaration of competing interest

The authors declare that they have no known competing financial interests or personal relationships that could have appeared to influence the work reported in this paper.

Data availability

Data will be made available on request.

Acknowledgments

We acknowledge support from the Agence Nationale de la Recherche (ANR, grant MCG-RAD ANR-18-CE46-0012, https://mcg-rad.ipsl.fr/).

Appendix. Spectro-radiative path-integral construction as a solution to the Radiative Transfer Equation

Starting from the monochromatic radiative transfer equation given by Eq. (3), expressed over the sightline $(\vec{x},\vec{u})$ parameterized by distance l, we have:

$$\frac{\partial L(\vec{x},\vec{u})}{\partial l} = -k_{ext}(\vec{x})L(\vec{x},\vec{u}) + k_a(\vec{x})L^{eq}(\vec{x}) + k_s(\vec{x})\int_{4\pi} p(\vec{u}',\vec{u})d\vec{u}'\,L(\vec{x},\vec{u}) \quad (13)$$

where the frequency-related subscript ν is removed for simplicity (all quantities are monochromatic).

Now, we introduce an upper-bound parameter $\hat{k}_{ext}$ of the extinction coefficient field k_{ext}, uniform over the whole domain Ω. Eq. (13) can be reformulated as:

$$\frac{\partial L(\vec{x},\vec{u})}{\partial l} = -\hat{k}_{ext}L(\vec{x},\vec{u}) + \hat{k}_{ext}S(\vec{x},\vec{u}) \quad (14)$$

with the following source term:

$$S(\vec{x},\vec{u}) = L(\vec{x},\vec{u}) + \frac{1}{\hat{k}_{ext}}\left[-k_{ext}(\vec{x})L(\vec{x},\vec{u}) + k_a(\vec{x})L^{eq}(\vec{x}) + k_s(\vec{x})\int_{4\pi} p(\vec{u}',\vec{u})d\vec{u}'\,L(\vec{x},\vec{u})\right] \quad (15)$$

If we further assume that $\hat{k}_{ext}$ is the sum of $\hat{k}_a$ and $\hat{k}_s$, upper-bound parameters for, respectively, the absorption coefficient field and the scattering coefficient field (these quantities are also uniform in Ω), the source term can be expressed as follows:

$$\begin{aligned} S(\vec{x},\vec{u}) = {} & \frac{\hat{k}_a}{\hat{k}_{ext}}\left[\frac{k_a(\vec{x})}{\hat{k}_a}L^{eq}(\vec{x}) + \left(1-\frac{k_a(\vec{x})}{\hat{k}_a}\right)L(\vec{x},\vec{u})\right] \\ & + \frac{\hat{k}_s}{\hat{k}_{ext}}\left[\frac{k_s(\vec{x})}{\hat{k}_s}\int_{4\pi} p(\vec{u}',\vec{u})d\vec{u}'\,L(\vec{x},\vec{u}) + \left(1-\frac{k_s(\vec{x})}{\hat{k}_s}\right)L(\vec{x},\vec{u})\right] \end{aligned} \quad (16)$$

Given that $\hat{k}_{ext}$ is uniform over Ω, Eq. (14) has a well known solution:

$$L(\vec{x},\vec{u}) = L^{\partial\Omega}(\vec{y},\vec{u})\exp\left(-\hat{k}_{ext}l_0\right) + \int_0^{l_0}\hat{k}_{ext}\exp\left(-\hat{k}_{ext}l\right)dl\left\{S(\vec{x}-l\vec{u},\vec{u})\right\} \quad (17)$$

with l_0 the distance between position $\vec{x}$ and the boundary, in direction $\vec{u}$. Firstly, the attenuation term between $\vec{x}$ and the boundary is replaced by $\int_{l_0}^{+\infty}\hat{k}_{ext}\exp\left(-\hat{k}_{ext}l\right)dl$. Secondly, making use of the Heaviside notation $\mathcal{H}$ and $\vec{x}' = \vec{x} - l\vec{u}$, the previous solution consisting of two separate integral terms is reformulated using a single integral:

$$\begin{aligned} L(\vec{x},\vec{u}) = {} & \int_0^{+\infty}\hat{k}_{ext}\exp\left(-\hat{k}_{ext}l\right)dl \\ & \times \left\{S(\vec{x}-l\vec{u},\vec{u})\mathcal{H}(\vec{x}'\in\Omega) + L^{\partial\Omega}(\vec{y},\vec{u})\mathcal{H}(\vec{x}'\notin\Omega)\right\} \end{aligned} \quad (18)$$

Introducing the source term from expression (16) into this integral form, we obtain:

$$\begin{aligned} L(\vec{x},\vec{u}) = {} & \int_0^{+\infty}\hat{k}_{ext}\exp\left(-\hat{k}_{ext}l\right)dl\left\{ L^{\partial\Omega}(\vec{y},\vec{u})\mathcal{H}(\vec{x}'\notin\Omega)\right. \\ & + \left[\frac{\hat{k}_a}{\hat{k}_{ext}}\left[\frac{k_a(\vec{x}')}{\hat{k}_a}L^{eq}(\vec{x}') + \left(1-\frac{k_a(\vec{x}')}{\hat{k}_a}\right)L(\vec{x}',\vec{u})\right]\right. \\ & \left.\left. + \frac{\hat{k}_s}{\hat{k}_{ext}}\left[\frac{k_s(\vec{x}')}{\hat{k}_s}\int_{4\pi} p(\vec{u}',\vec{u})d\vec{u}'\,L(\vec{x}',\vec{u}') + \left(1-\frac{k_s(\vec{x}')}{\hat{k}_s}\right)L(\vec{x}',\vec{u})\right]\right] \\ & \left.\times\ \mathcal{H}(\vec{x}'\in\Omega)\right\} \end{aligned} \quad (19)$$

Moreover, according to a line-by-line approach, the absorption coefficient at a given frequency ν is formalized as the sum of the contributions of N_t transitions, for the same frequency: $k_a(\vec{x}) = \sum_{j=1}^{N_t} h_{a,j}$.

We further introduce an upper-bound parameter, noted $\hat{h}_{a,j}$, to the contribution of each transition j to the total absorption coefficient (this upper-bound value is also uniform within Ω), which makes possible to reformulate $\frac{k_a(\vec{x})}{\hat{k}_a}$ as $\sum_{j=1}^{N_t} \frac{\hat{h}_{a,j}}{\hat{k}_a} \frac{h_{a,j}(\vec{x})}{\hat{h}_{a,j}}$ and $1-\frac{k_a(\vec{x})}{\hat{k}_a}$ as $\sum_{j=1}^{N_t} \frac{\hat{h}_{a,j}}{\hat{k}_a}\left(1-\frac{h_{a,j}(\vec{x})}{\hat{h}_{a,j}}\right)$; the integral solution thus reads:

$$
\begin{aligned}
L(\vec{x},\vec{u}) = \int_0^{+\infty} \hat{k}_{ext} \exp\left(-\hat{k}_{ext} l\right) dl \Bigg\{ & L^{\partial\Omega}(\vec{y},\vec{u}) \mathcal{H}(\vec{x}' \notin \Omega) \\
& + \Bigg[\frac{\hat{k}_s}{\hat{k}_{ext}} \Big[\frac{k_s(\vec{x}')}{\hat{k}_s} \int_{4\pi} p(\vec{u}',\vec{u}) d\vec{u}' L(\vec{x}',\vec{u}') + \left(1-\frac{k_s(\vec{x}')}{\hat{k}_s}\right) L(\vec{x}',\vec{u}) \Big] \\
& + \frac{\hat{k}_a}{\hat{k}_{ext}} \Big[\sum_{j=1}^{N_t} \frac{\hat{h}_{a,j}}{\hat{k}_a} \Big[\frac{h_{a,j}(\vec{x}')}{\hat{h}_{a,j}} L^{eq}(\vec{x}') + \left(1-\frac{h_{a,j}(\vec{x}')}{\hat{h}_{a,j}}\right) L(\vec{x}',\vec{u}) \Big] \Big] \Bigg] \\
& \times \mathcal{H}(\vec{x}' \in \Omega) \Bigg\}
\end{aligned}
\tag{20}
$$

In terms of the Monte Carlo algorithm associated to this path-integral formulation, we define the following quantities:

- $\hat{P}_s = \frac{\hat{k}_s}{\hat{k}_{ext}}$ is the probability to retain the "scattering" branch of the algorithm;
- $\frac{\hat{k}_a}{\hat{k}_{ext}}$ is the complementary probability, noted $1-\hat{P}_s$, is the probability to retain the "absorption" branch of the algorithm;
- $P_s(\vec{x}) = \frac{k_s(\vec{x})}{\hat{k}_s}$ is the probability a scattering event is retained. The complementary probability $1-\frac{k_s(\vec{x})}{\hat{k}_s}$ is the probability a "null scattering" event is sampled;
- $P_J(j) = \frac{\hat{h}_{a,j}}{\hat{k}_a}$ is the probability to sample transition of index j among N_t transitions, for current frequency ν;
- $P_{a,j}(\vec{x}) = \frac{h_{a,j}(\vec{x})}{\hat{h}_{a,j}}$ is the probability a real absorption event is sampled, and the complementary probability $1-\frac{h_{a,j}(\vec{x})}{\hat{h}_{a,j}}$ is the probability a "null absorption" event is sampled.

With these notations, the integral formulation of the general solution to the radiative transfer equation finally reads:

$$
\begin{aligned}
L(\vec{x},\vec{u}) = \int_0^{+\infty} \hat{k}_{ext} \exp\left(-\hat{k}_{ext} l\right) dl \Bigg\{ & L^{\partial\Omega}(\vec{y},\vec{u}) \mathcal{H}(\vec{x}' \notin \Omega) \\
& + \Bigg[\hat{P}_s \Big[P_s(\vec{x}) \int_{4\pi} p(\vec{u}',\vec{u}) d\vec{u}' L(\vec{x}',\vec{u}') + \left(1-P_s(\vec{x})\right) L(\vec{x}',\vec{u}) \Big] \\
& + \left(1-\hat{P}_s\right) \Big[\sum_{j=1}^{N_t} P_J(j) \Big[P_{a,j}(\vec{x}) L^{eq}(\vec{x}') + \left(1-P_{a,j}(\vec{x})\right) L(\vec{x}',\vec{u}) \Big] \Big] \Bigg] \\
& \times \mathcal{H}(\vec{x}' \in \Omega) \Bigg\}
\end{aligned}
\tag{21}
$$

which is identical to Eq. (5).

References

[1] Pincus R, et al. Computational cost and accuracy in calculating three-dimensional radiative transfer : Results for new implementations of Monte Carlo and SHDOM. J Atmos Sci 2009;66(10):3131–46.

[2] Mayer B. Radiative transfer in the cloudy atmosphere. Eur Phys J Conf 2009;1:75–99.

[3] Niro F, et al. European space agency (ESA) calibration/validation strategy for optical land-imaging satellites and pathway towards interoperability. Remote Sens 2021;13(15):3003.

[4] Schwaerzel M, et al. Impact of 3D radiative transfer on airborne NO_2 imaging remote sensing over cities with buildings. Atmos Meas Tech 2021;14(10):6469–82.

[5] Villefranque N, et al. A path-tracing Monte Carlo library for 3-d radiative transfer in highly resolved cloudy atmospheres. J Adv Modelling Earth Syst 2019;11(8):2449–73.

[6] Tregan J-M, et al. Coupling radiative, conductive and convective heat-transfers in a single Monte Carlo algorithm: A general theoretical framework for linear situations. PLoS One 2023;18(4):e0283681.

[7] Ibarrart L, et al. Advection, diffusion and linear transport in a single path-sampling Monte Carlo algorithm : getting insensitive to geometrical refinement, working paper or preprint : https://hal.science/hal-03818899v2/file/main%20%281%29.pdf.

[8] Villefranque N, et al. The teapot in a city : A paradigm shift in urban climate modeling. Sci Adv 2022;8(27).

[9] Galtier M, et al. Radiative transfer and spectroscopic databases : A line-sampling Monte Carlo approach. J Quant Spectrosc Radiat Transfer 2016;172:83–97.

[10] Nyffenegger-Péré Y. Coupler le rayonnement et la spectroscopie raie par raie dans un même algorithme de Monte Carlo : permettre le calcul de référence des forçages radiatifs (Ph.D. thesis), Paul Sabatier University, [submitted for publication].

[11] Novák J, et al. Monte Carlo methods for volumetric light transport simulation. In: Computer graphics forum (proceedings of eurographics - state of the art reports). 2018.

[12] Miller B, et al. A null-scattering path integral formulation of light transport. In: ACM transactions on graphics (Proceedings of SIGGRAPH). 2019.

[13] McCool MD, et al. Probability trees. In: Proceedings of the conference on graphics interface. 1997.

[14] Nyffenegger-Péré Y, et al. Spectrally refined unbiased Monte Carlo estimate of the Earth's global radiative cooling. Proc Natl Acad Sci 2024;121(5):e231549212.

[15] de Lataillade A, et al. Monte Carlo method and sensitivity estimations. J Quant Spectrosc Radiat Transfer 2002;75(5):529–38.

[16] Zeltner T, et al. Monte Carlo estimators for differential light transport. ACM Trans Graph 2021;40(4):1–16.

[17] Tregan J-M, et al. Convergence issues in derivatives of Monte Carlo null- collision integral formulations : A solution. J Comput Phys 2020;413:109463.

[18] Lapeyre P, et al. Monte Carlo and sensitivity transport models for domain deformation. J Quant Spectrosc Radiat Transfer 2020;251:107022.

[19] Lapeyre P, et al. A physical model and a Monte Carlo estimate for the specific intensity spatial derivative, angular derivative and geometric sensitivity, working paper or preprint : https://arxiv.org/abs/2206.05167.

[20] Pincus R, et al. Benchmark calculations of radiative forcing by greenhouse gases. J Geophys Res: Atmos 2020;125(23):e2020JD033483.

[21] Ogura T, et al. Importance of instantaneous radiative forcing for rapid tropospheric adjustment. Clim Dyn 2013;43.

[22] El Hafi M, et al. Three viewpoints on null-collision Monte Carlo algorithms. J Quant Spectrosc Radiat Transfer 2021;260:107402.

[23] Maire S, et al. Stochastic finite differences for elliptic diffusion equations in stratified domains. Math Comput Simulation 2016;121:146–65.

[24] Bossy M, et al. Monte Carlo methods for linear and non-linear Poisson–Boltzmann equation. ESAIM: Proc Surv 2015;48:420–46.

[25] Galtier M, et al. Integral formulation of null-collision Monte Carlo algorithms. J Quant Spectrosc Radiat Transfer 2013;125:57–68.

[26] Terrée G, et al. Addressing the gas kinetics Boltzmann equation with branching-path statistics. Phys Rev E 2022;105(2):025305.

[27] Boucher O, et al. Presentation and evaluation of the IPSL-CM6a-LR climate model. J Adv Modelling Earth Syst 2020;12(7):e2019MS002010.

[28] Gordon Iouli E, et al. The HITRAN2020 molecular spectroscopic database. J Quant Spectrosc Radiat Transfer 2022;277:107949.

[29] Farges O, et al. Life-time integration using Monte Carlo methods when optimizing the design of concentrated solar power plants. Sol Energy 2015;113.

[30] IPCC. In: Houghton JT, Jenkins GJ, Ephraums JJ, editors. Climate change: the IPCC scientific assessment. Published by Cambridge University Press; 1980, p. 365.

[31] Jeevanjee N, et al. An analytical model for spatially varying clear-sky CO_2 forcing. J Clim (J Clim) 2021;34(23).